JOURNAL OF MATERIALS SCIENCE **35** (2000) 1629–1639

A filiform corrosion and potentiodynamic polarisation study of some aluminium alloys

J. M. C. MOL
Laboratory of Materials Science, Delft University of Technology, Rotterdamseweg 137, NL-2628 AL Delft, The Netherlands
E-mail: J.M.C.Mol@tnw.tudelft.nl

B. R. W. HINTON
Aeronautical and Maritime Research Laboratory, Defence Science and Technology Organisation, PO Box 4331, Melbourne, Victoria 3001, Australia

D. H. VAN DER WEIJDE, J. H. W. DE WIT, S. VAN DER ZWAAG
Laboratory of Materials Science, Delft University of Technology, Rotterdamseweg 137, NL-2628 AL Delft, The Netherlands

The aim of the present investigation is a combined study of filiform corrosion of aluminium alloys by accelerated exposure tests and potentiodynamic polarisation measurements. The accelerated exposure tests are performed on binary Al-Cu, Al-Mg, Al-Si and Al-Zn model alloys, a ternary Al-MgSi alloy and on the two commercial alloys, AA2024-T351 and AA7075-T651, with variations of composition and surface treatments. The surface treatments cover simple degreasing, chromate and cerium based treatments. A trend of a higher filiform corrosion susceptibility with increasing alloying elements concentrations was observed for all model systems. Furthermore, the filiform corrosion susceptibility varies with the solute atom, in particular Cu was found to have a detrimental effect on the filiform corrosion properties. Both chromating and cerating improve the filiform corrosion resistance of the alloys significantly. To explain the trends observed in the exposure tests, polarisation measurements were performed on the untreated Al-Cu and Al-Zn alloys in bulk anolyte and catholyte solutions which are characteristic for the local anodic and cathodic sites in the filaments on the aluminium substrates. From these measurements a filiform corrosion current, defined as the intercept of the anodic and cathodic curves, can be determined. The present set of experiments shows a correlation between the filiform corrosion properties during accelerated exposure tests and the potentiodynamic polarisation measurements for the Al-Cu alloys. When comparing the results for the Al-Cu and Al-Zn binary alloys it can be concluded that the correlation factor differs significantly with the solute atom and the filiform corrosion current proves to be a non-uniquely discriminating parameter for the filiform corrosion susceptibility of the model alloys. The difference in correlation factor for the Al-Cu and Al-Zn alloys is attributed to differences in the electrochemical behaviour of these alloys with local variations in substrate composition. For the Al-Cu and Al-Zn model alloys the filiform corrosion initiation characteristics are related to the passive range and thus implicitly to the ease of pitting of the alloy. A smaller passive range corresponds to a higher filiform site density for both the Al-Cu and Al-Zn alloys.

1. Introduction

Filiform corrosion is a type of local corrosive attack on a metal substrate covered by an organic coating and is characterised by thread-like tracks. It occurs on aluminium alloys, but also on steel and magnesium based substrates. The local attack is a complex phenomenon involving influences of the environmental conditions, the organic coating, the coating-substrate interface and the substrate surface. Due to the many parameters involved, the relevant factors for filiform corrosion have not been established unambiguously [1].

Aim of the present investigation is the determination of the effect of microstructural variations in aluminium based substrates on the filiform corrosion properties. The composition and structure of the surface layer/oxide is strongly influenced by the local

composition of the underlying aluminium alloy. Especially precipitates and dispersoids with microscopical dimensions can influence the composition and structure of this surface layer/oxide [2]. The composition and morphology of the constituent particles are a function of the thermomechanical treatments during the preceding production steps such as casting, solidification, homogenisation, extrusion and precipitation.

Traditionally, local corrosion processes have been attributed to successive interactions between the alloy matrix and clustered particles [3, 4]. Local breakdown of the surface film permits subsequent local dissolution of the metallic substrate [5–7]. Such an explanation is implicitly supported by the absence of reports on filiform corrosion on superpure aluminium. Recent studies [8–12] of particle-induced corrosion indicate that the electrochemical characters of constituent particles can vary and may be broadly divided into particles which are cathodic or anodic with respect to the aluminium matrix. Observations [8, 9] show that anodic particles are likely to be dissolved preferentially, whereas cathodic particles tend to promote dissolution of the surrounding matrix. The characterisation of these particles in this manner, however, is not precise. Because of redeposition of relatively cathodic metallic phases, such as Cu, from anodic particles back onto the (anodic and cathodic) constituent particles during corrosion, most of the particles tend to behave cathodically and promote matrix dissolution. However, very little systematic research into the effects of variations of the composition and microstructure of aluminium alloys on the filiform corrosion properties has been performed. To study the effect of single alloying additions of Si, Mg, Cu and Zn, eleven binary model aluminium alloys have been investigated during the present research. In addition, one ternary Al-MgSi model alloy and the two typical aircraft aluminium alloys AA2024-T351 and AA7075-T651 have been investigated.

As filiform corrosion not only depends on the substrate but also on the coating and on the surface pretreatment [1], these factors were kept constant or were set to three very different levels respectively. By choosing an air-drying coating system, microstructural changes taking place during curing at elevated temperatures can be avoided and the effect of the microstructure in its as delivered state can be determined. When examining the effect of surface pretreatment both a minimal but reproducible pretreatment (controlled degreasing) and technically well proven pretreatments are of particular interest. Chromate conversion coatings are commonly used on aluminium based surfaces in order to improve the corrosion resistance of the metal and establish an adhesive base for organic coatings [13]. The chromate ion is an excellent corrosion inhibitor and is widely used for chromate conversion coatings and in paint pigments. However, it has been recognised for some time that chromates are both highly toxic and carcinogenic [14]. As a result of this toxicity, the concentration levels of chromate allowed in the workplace are now regulated by government agencies and users of chromate containing materials are being warned of the possible health dangers. An interesting modern alternative chromium free chemical treatment, using solutions containing cerium compounds [15–18], has been reported to be successful in the prevention of localised corrosion of aluminium and its alloys. The positive effect of cerium has been attributed to the inhibition of reduction reactions at cathodic sites, due to the formation of a protective cerium oxide layer on top of the aluminium substrate [19–22]. While a detailed examination of the filiform corrosion rate as a function of the substrate composition and the surface pretreatment applied yields valuable results, it does not provide explanations for observed dependencies. The underlying mechanisms for filiform corrosion can only be found by performing electrochemical measurements in media characteristic for the corrosion process studied. To this aim potentiodynamic polarisation measurements in synthetic anolyte and catholyte media are performed on six of the most interesting alloy systems.

2. Theoretical background

Potentiodynamic polarisation measurements are performed in bulk anolyte and catholyte solutions which are characteristic for local anodic and cathodic sites in filaments on aluminium substrates, resulting from the differential aeration and subsequent anodic undermining [1, 23], as presented in Fig. 1. The differential aeration results in spatial separation of the anodic site in the active tip of the filament, where aluminium dissolves, and the cathodic site at the passive trailing area, where oxygen is reduced to produce hydroxyl ions. The anodic and cathodic sites are spatially separated by a poorly defined membrane, similar to the membrane of solid corrosion products reported by Van der Weijde *et al.* [24] for cathodic delamination on iron based substrates. Chloride ions are essential to provide electrolyte conductivity and to stimulate the initiation of corrosion and these ions migrate with the filament head and are only partially incorporated in the hydrated corrosion products in the filament tail. Initial investigations on

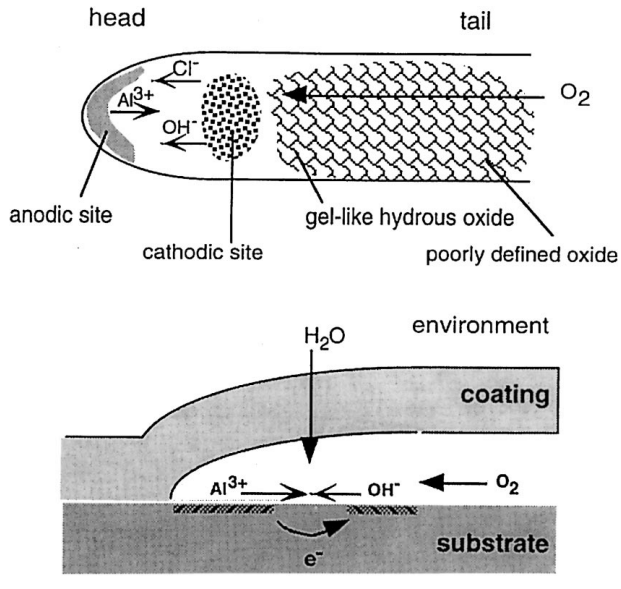

Figure 1 The propagation of filiform corrosion on aluminium according to the anodic undermining mechanism [1].

extruded AA1050 alloys with the use of a macro differential aeration cell by Lobry *et al.* [25], mainly focussing on the effect of variations of electrolyte pH and chloride concentrations, confirm the differential aeration principle for filiform corrosion on aluminium. The theoretical background of the combined study of accelerated exposure tests and potentiodynamic polarisation measurements is briefly discussed here. A more detailed and fundamental correlation is presented by Huisert *et al.* [26].

The anodic dissolution reaction of aluminium in the presence of chloride ions is [27]:

$$Al + 2H_2O + Cl^- \rightarrow Al(OH)_2Cl + 2H^+ + 3e^- \quad (1)$$

Due to the acidity at the anodic site also hydrogen evolution takes place as a secondary cathodic reaction:

$$2H^+ + 2e^- \rightarrow H_2(g) \quad (2)$$

Also in this work the evolution of gas bubbles in the filament tip has been observed. In line with the literature [28, 29] and Equation 2 these bubbles are taken to be hydrogen bubbles. The main cathodic reaction at the cathodic site will be the reduction of oxygen:

$$O_2 + 2H_2O + 4e^- \rightarrow 4OH^- \quad (3)$$

The number of electrons produced by the anodic dissolution should be equal to the number of electrons consumed by the cathodic reactions. The net production of electrons at the anodic site, i.e. resulting from the aluminium dissolution and hydrogen reduction reactions, is consumed at the spatially separated cathodic site. This electronic current is equal to the net ionic current through the electrolytes and in this paper defined as the filiform corrosion current. Following the basic principles of the mixed-potential theory [30], this filiform corrosion current can be derived from the potentiodynamic polarisation measurements by determination of the intercept of the anodic part of the polarisation curve in the anolyte and the cathodic part of the polarisation curve in the catholyte, assuming a certain effective cathode/anode area ratio. The electrolytical resistance between the anodic and cathodic sites in real filaments is therefore not taken into account in the potentiodynamic polarisation measurements. In the present investigation this filiform corrosion current is related to the filiform corrosion properties during the accelerated exposure tests. A relatively high filiform corrosion current implies a relatively high number of electrons produced at the anodic site as a result of the anodic aluminium dissolution reaction, according to (1). The local morphology of corrosion attack within the filament may vary with alloy composition and pretreatment. During the present investigation the filiform corrosion current is related to one-dimensional propagation properties of the filaments. Filament width and in-depth attack are considered to be similar and constant for comparable systems. Consequently, according to this theory, a relatively high filiform corrosion current should correlate with a higher filiform growth rate. As the exact anolyte and catholyte compositions are still unkown, the following considerations have been used as a basis for the formulation of electrolytes for potentiodynamic polarisation measurements.

Slabaugh [28] and Hoch [31] have reported the acidity in the filament tip to be at a pH of 1 to 2. During the present investigation these low pH values are confirmed by opening a filament by scalpeling around a filament through the organic coating, lifting the coating, immediately followed by testing the electrolyte in the filament tip by narrow range pH indicator paper. Slabaugh [28] also reported the presence of chlorides in the filament tip and also during the present investigation qualitative SEM/EDX analysis of filaments gave evidence of high chloride concentrations at the very tips of filaments. Due to the anodic dissolution of aluminium, also aluminium ions should be present. Finally, according to the differential aeration theory [1, 23], the oxygen concentration at the anodic site is expected to be very low, as the oxygen diffuses mainly through the tail of the filament and is reduced just behind the anodic site. The catholyte is assumed to be alkaline as a result of the reduction of oxygen at the cathodic site. Both the exact value of the pH of the catholyte and the effective cathode/anode area ratio are hard to determine in practice because of the low liquidity just behind the tip.

3. Experimental

Eleven binary and one ternary cold-rolled aluminium model alloys are examined. The composition and alloy codes are listed in Table I. All alloys have been DC cast as 20 × 7.5 cm blocks on a 99.998% base, scalped, homogenised 16 h at 465 °C, hot-rolled to 15–20 mm, reheated 1 h at 465 °C, hot rolled to 6 mm, cold-rolled to 4 mm, solution heat treated at 550/650 °C followed by a cold water quench, cold rolled to 1.1–1.2 mm and flattened in a hot press at 225 °C pressing plate temperature for 12 mins. The dimensions of the specimens are $L \times LT \times T = 70$ mm × 60 mm × 1.1–1.2 mm. In addition, two typical aircraft aluminium alloys AA2024-T351 and AA7075-T651 are studied. The dimensions of these specimens are $L \times LT \times T = 76$ mm × 128 mm × 1.6 mm.

For each of the alloys, the following pretreatments were applied prior to coating with polyurethane. It is important to note that none of the conditions of

TABLE I Composition and alloy code of binary and ternary model alloys

Alloying element	Alloying concentration [wt-%]	Alloy code
Si	0.11	Al-0.11Si
	0.21	Al-0.21Si
	4.07	Al-4.07Si
Mg	0.44	Al-0.44Mg
	3.06	Al-3.06Mg
Mg and Si	2.46 Mg and 1.40 Si	Al-2.46Mg1.40Si
Cu	0.20	Al-0.20Cu
	1.00	Al-1.00Cu
Zn	0.19	Al-0.19Zn
	0.48	Al-0.48Zn
	0.97	Al-0.97Zn
	2.09	Al-2.09Zn

All model alloys are based on 99.998% Al.

application of these pretreatments had been optimised for maximum corrosion protection and coating adhesion before the study commenced. Prior to the surface treatment, all alloys are carefully cleaned with ethanol.

3.1. Degreasing

Immersion for 10 minutes in Brulin Formula 815 GD (alkaline cleaner) at 60°C, followed by a cold water rinse in running tap water for 5 minutes.

3.2. Chromate conversion coating

A second set of specimens are chromated according to the following procedure:

— Degreasing in Brulin Formula 815GD, as above.
— Degreasing by immersion for 4 minutes in Parker Amchem Ridoline 53 (silicated alkaline cleaner), followed by a cold water rinse for 2 minutes.
— Deoxidisation by immersion for 10 minutes in Parker Amchem Deoxidiser #4 at room temperature, followed by a cold water rinse for 2 minutes.
— Chromate conversion coating by immersion in a 'Alodine 1200' solution in accordance with product data sheets, followed by a cold water rinse for 5 minutes. For all systems the chromating time was set to 2 minutes except for the technical alloys and the Al-Cu alloys which were chromated for 1 minute.

3.3. Cerate conversion coating

The third set of samples are cerated [19] according to the following procedure:

— Degreasing and deoxidisation as above for chromate conversion coating.
— Cerating at pH 2.00 ± 0.05 at 45°C by immersion, followed by cold water rinse for 5 minutes. For all alloys the cerating time was set to 5 minutes except for the commercial alloys and the Al-Cu alloys which were cerated for 1 minute.

Following the pretreatment, an air-drying clear flexible polyurethane coating was spray deposited in two stages with a mean dry coating thickness of 42 μm in total (standard deviation 4 μm). The coating defect was applied by scribing perpendicular to the rolling direction with a scalpel, just before the initiation procedure.

The filiform corrosion test was carried out according to specification DIN65472 [32], with the modification of an initiation time above hydrochloric acid vapour of only 15 minutes instead of 1 hour. The total exposure time was 1000 hours. The degree of filiform corrosion was then determined using optical microscopy for quantifying the density and average length of the filaments. A manual procedure was used to determine the characteristics data but good care was taken in standardizing the evaluation. Per model alloy investigated, a total scratch length of 50 mm for the degreased samples and 100 mm for the chromated and cerated samples was examined. For the AA2024-T351 and AA7075-T651 the total examined scratch length was 100 mm for the degreased samples and 200 mm for the chromated and cerated samples. Both sides of the scratch were treated seperately. The filiform corrosion initiation characteristics are defined as the site density which is the number of filaments per scratch length. The propagation properties are defined by the average filament length per specimen, with a resolution of 0.5 mm. The total attack is defined as the corrosion number and is equal to the site density multiplied by the average filament length.

As discussed in the theoretical background of the present combined study and the investigations of Huisert *et al.* [26], the exact anolyte and catholyte compositions have not been reported in the literature yet. However, in the literature pH values of 1–2 [28, 31] and high chloride concentrations [28] in the very filament tips are reported, which are confirmed during the present investigation. Furthermore, due to the anodic dissolution of aluminium, aluminium ions should be present at the anodic site and following the differential aeration theory [1, 23], the oxygen concentration at the anodic site is expected to be very low. Following these considerations the potentiodynamic polarisation measurements typical for the anodic site are performed in the following anolyte: 0.86 M $NaCl + 0.1$ M $AlCl_3$, acidified to pH 2 with concentrated HCl (33%) and actively deaerated with high purity nitrogen gas. The catholyte is assumed to be alkaline as a result of the reduction of oxygen and water at the cathodic site, as presented in Equation 3. Assuming total electroneutrality for a filament in dynamic equilibrium and an effective cathode/anode area ratio of 100, the polarisation measurements in the catholyte are conducted in a solution of distilled water adjusted to pH 10 by addition of NaOH and actively aerated with air, to ensure a constant and fixed oxygen concentration during the potentiodynamic polarisation measurements.

The electrochemical cell consisted of an Avesta cell [33], the aluminium based alloy as a working electrode (working area 0.8 cm^2), a commercial saturated calomel electrode (SCE) and a platinum cylindrical small-mesh wire netting counter electrode. Prior to the electrochemical measurements the specimens are degreased with ethanol and Brulin 815 GD. The open circuit potential (OCP) of the system was allowed to come to equilibrium over a 5 hour period before the commencement of the polarisation scans. Even though some corrosion did occur during this period, the time at the OCP prior to testing did ensure that the system was stable, enabling proper potentiodynamic polarisation measurements at a stable OCP on a surface representative of an active anodic or cathodic site in a filament. The scan rate for the potentiodynamic polarisation experiments was 0.2 mV/sec and were started at cathodic potentials. The scans in the anolyte were started at -100 mV vs. OCP to $+200$ mV vs. OCP; in the catholyte the scans were started at -200 mV vs. OCP to $+100$ mV vs. OCP. The potentiodynamic polarisation scans were carried out at room temperature using a PAR273A potentiostat.

The combined filiform corrosion and electrochemical study is validated by analysing both highly and less filiform corrosion susceptible substrates. For these reasons both the Al-Cu and Al-Zn model alloys are studied

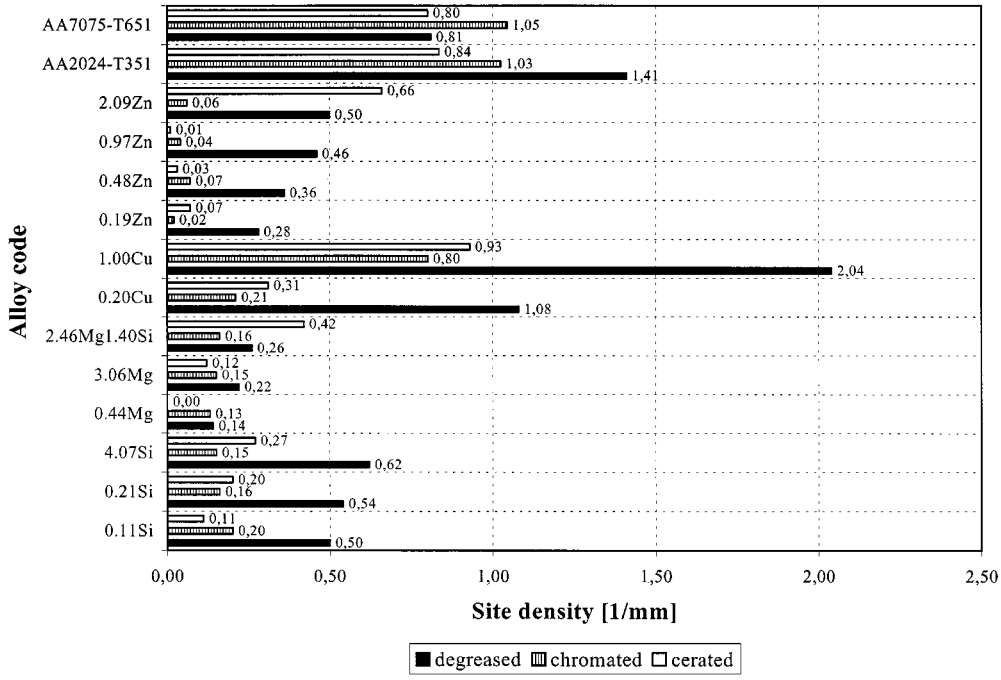

Figure 2 Site density after 1000 hours of accelerated filiform corrosion test exposure for three pretreatments. The alloy codes are listed in Table I.

both on their filiform corrosion properties and their potentiodynamic polarisation response. Only degreased samples are analysed during the present combined study to ensure that the compositional variations in the substrates are the only variables to dedicate the variations in the potentiodynamic polarisation response.

4. Results and discussion

For all binary, ternary and commercial aluminium alloys the values of the site density, average filament lengths and corrosion numbers after 1000 hours of accelerated exposure are presented in Figs 2, 3 and 4. In all experiments filiform corrosion behaviour was observed except in the case of the experiments on degreased AA2024-T351 and AA7075-T651, where a form of front corrosion was observed and the calculated filiform corrosion characteristics are rough indications only.

4.1. Site density

Fig. 2 indicates large differences in filament site density between the various alloy systems and surface pretreatments. A maximum site density of ∼2 filaments per mm was obtained for the degreased Al-1.00Cu alloy, whereas a minimum site density down to ∼0.01 per mm was obtained for chromated and cerated Al-Zn alloys. When evaluating the site density data of the binary alloy system it is clear that the average site density decreases in the order Al-Cu, Al-Si, Al-Zn, Al-Mg. The trend is more or less independent of the surface pretreatment applied, however the chromated and cerated Al-Zn alloys show an exceptionally good resistance to filiform initiation, with the exception of the cerated Al-2.09Zn alloy. The reason for this not known yet and is subject of further study. A further observation is that for each binary alloy system the site density increases with increasing solute content. This trend is particularly clear for the degreased samples. For the chromated and cerated samples the site density was too low to determine such a relation with any statistical significance but the data would not contradict such a conclusion. Chromating proves to be a very effective way to reduce the filiform corrosion initiation characteristics significantly for all tested substrates. There is still some attack on the chromated AA2024-T351, AA7075-T651 and the Al-Cu binary alloys, but it has to be realized that these samples have only been chromated for 1 minute, compared to the others which have been chromated for 2 minutes. The effectiveness of cerating is expressed in a lower site density for all tested substrates with the exception of the Al-2.09Zn and the ternary Al-2.46Mg1.40Si alloys. The pretreated AA2024-T351 and AA7075-T651 alloys show equivalent filiform initiation susceptibility with site densities of ∼1.05 and ∼0.85 filaments per mm for the chromated and cerated samples respectively.

4.2. Average filament length

When analysing the average filament lengths for the model alloys, it can be concluded that the highest average filament lengths are obtained for the Al-Cu binary alloys. The other model alloys are far less susceptible to filiform corrosion propagation with average filament lengths all smaller than 1.32 mm, compared to 2.84 and 7.78 mm for the degreased Al-0.20Cu and Al-1.00Cu alloys respectively. The trend of an increasing average filament length with the alloying concentration is especially clear for the highly susceptible Al-Cu binary alloys and also for the degreased Al-Si alloys. This in contrast with the degreased Al-Zn and Al-Mg alloys which show no or little significant increase in average filament length with solute content. Generally, chromating also proves to be very effective in reducing the filiform corrosion propagation properties of the tested substrates. Besides the highly susceptible Al-Cu alloys, the Al-3.06Mg and the technical alloys, all other model alloys had no or only filaments smaller than 0.5 mm

after chromating. For the chromated binary alloys the average filament length was too low to determine a relation between the alloying concentration and the filiform corrosion propagation. All model and technical alloys still show significant filiform corrosion propagation, i.e. average filament lengths $\geq$0.5 mm, after cerating with the exception of the Al-0.44Mg alloy. No clear relation between the alloying concentration and filiform corrosion propagation can be determined for the cerated binary alloys, except for the highly susceptible Al-Cu binary alloys. Although the average filament lengths for the degreased AA2024-T351 and AA7075-T651 alloys presented in Fig. 3 are only qualitative indications, a higher front corrosion length can be observed for the degreased AA2024-T351 compared to the degreased AA7075-T651. A decrease in average filament length, i.e. front corrosion length for the degreased samples, can be observed after chromating or cerating of the AA2024-T351 alloy.

4.3. Corrosion number

Fig. 4 indicates large differences in the corrosion number between the various alloy systems and surface pretreatments. A maximum corrosion number of $\sim$16 was obtained for the Al-1.00Cu alloy, whereas for the cerated Al-0.44Mg alloy no filiform corrosion attack was found after the 1000 hours accelerated filiform

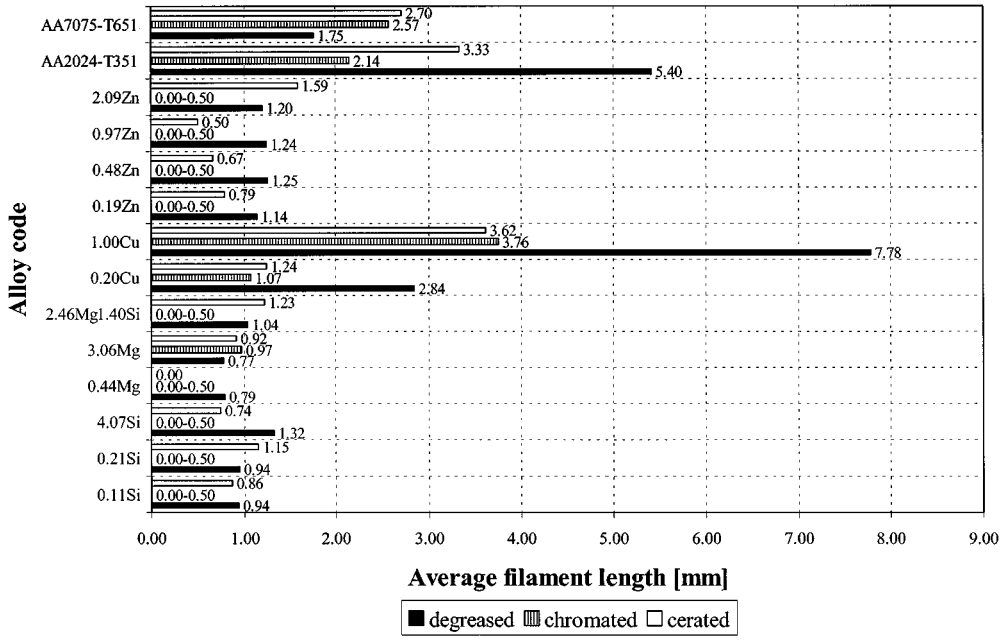

Figure 3 Average filament length after 1000 hours of accelerated filiform corrosion test exposure for three pretreatments. The alloy codes are listed in Table I.

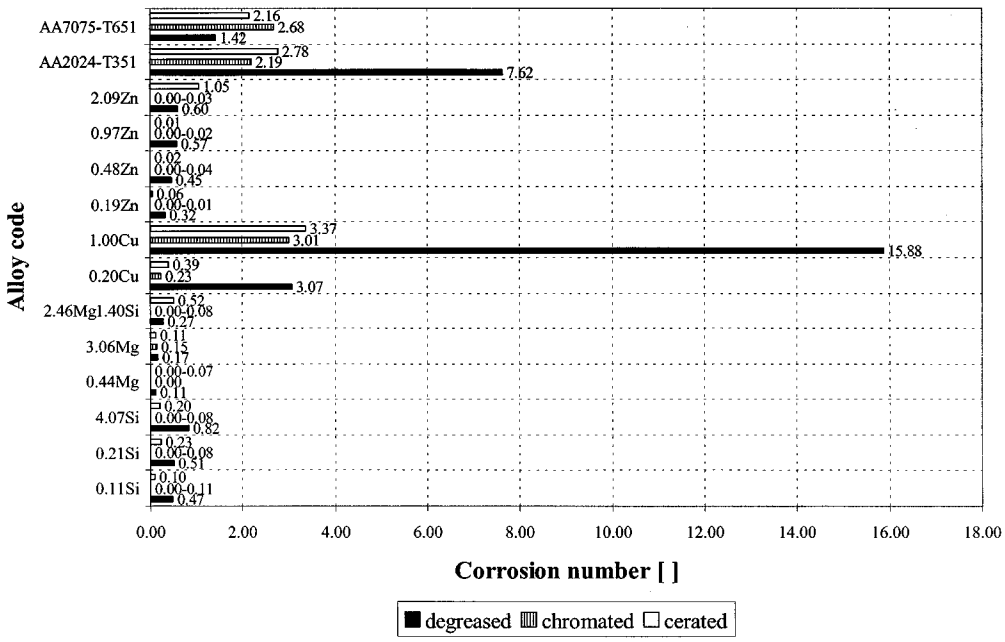

Figure 4 Corrosion number after 1000 hours of accelerated filiform corrosion test exposure for three pretreatments. The alloy codes are listed in Table I.

corrosion test. When evaluating the corrosion number data of the binary alloy system it is evident that the average corrosion number decreases in the order Al-Cu, Al-Si, Al-Zn, Al-Mg. A further observation is that per binary alloy system the corrosion number increases with the alloying concentration which is in line with observations presented in the literature [34, 35]. This trend is particularly clear for the degreased samples. On the chromated and cerated samples the filiform corrosion attack was too small to confirm such a relation with any statistical significance, but the data would not contradict such a conclusion. The detrimental effect of Cu as an alloying element in aluminium is very obvious for this set of experiments. The degreased AA2024-T351 show significantly more filiform corrosion attack compared to the AA7075-T651 alloy, with indicative corrosion numbers of 7.62 and 1.42 respectively. The chromate conversion coating results in a slightly lower corrosion number for the AA2024-T351, compared to the AA7075-T651, whereas the cerate conversion coating results in a slightly lower corrosion number for the AA7075-T651, compared to the AA2024-T351. Generally, the corrosion number for the chromated and cerated technical alloys only vary from 2.16 for the cerated AA7075-T651 to 2.78 for the cerated AA2024-T351.

4.4. Potentiodynamic polarisation measurements

For the degreased Al-Cu and Al-Zn binary alloys the characteristic potentiodynamic polarisation scans in both the anolyte and the catholyte are shown in Fig. 5a and b respectively. The characteristic potentials and the filiform corrosion currents derived from the potentiodynamic polarisation measurements arelisted in Table II.

TABLE II Summary of the characteristic potential and filiform corrosion current values for the Al-Cu and Al-Zn model alloys under anolyte and catholyte conditions

Alloy Code	Open circuit potential vs. SCE [V]		Pitting potential vs. SCE [V]	Passive range [V]	Filiform corrosion current [A]
	Anolyte	Catholyte	Anolyte	Anolyte	
Al-0.20Cu	−0.80	−0.77	−0.74	0.06	2.6×10^{-6}
Al-1.00Cu	−0.75	−0.64	−0.73	0.02	2.0×10^{-5}
Al-0.19Zn	−0.93	−0.87	−0.80	0.13	4.7×10^{-6}
Al-0.48Zn	−0.92	−0.77	−0.85	0.07	1.7×10^{-5}
Al-0.97Zn	−0.96	−0.78	−0.90	0.06	2.9×10^{-5}
Al-2.09Zn	−0.97	−0.84	−0.97	0.00	3.9×10^{-5}

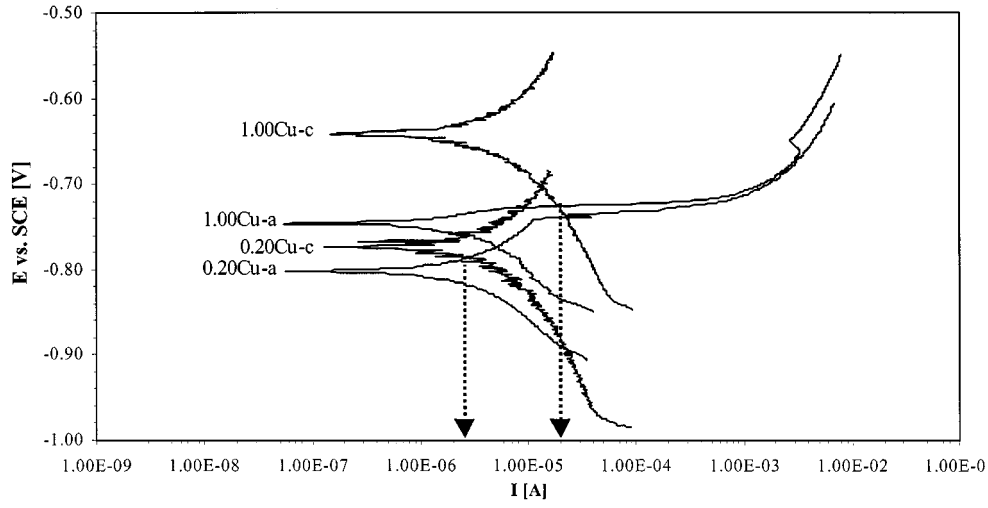

(a)

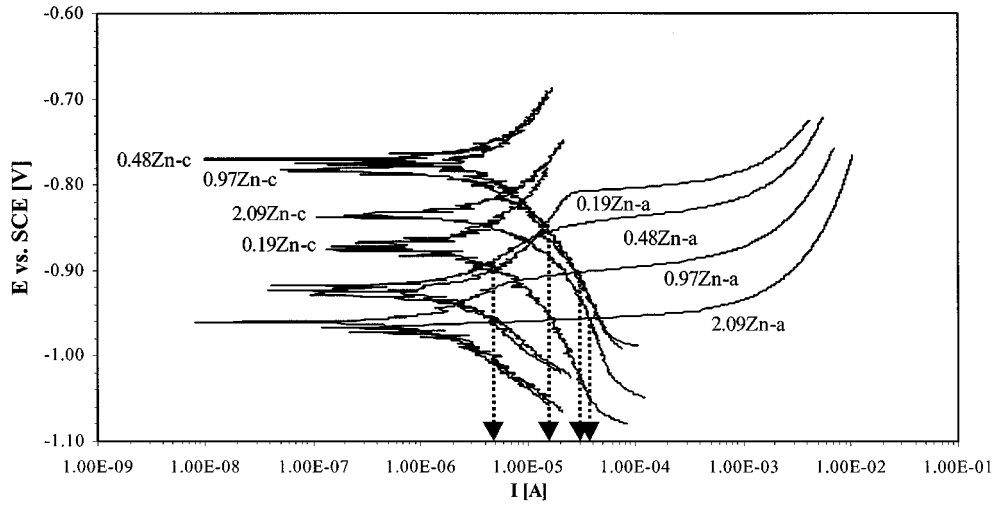

(b)

Figure 5 Typical potentiodynamic polarisation measurements for the Al-Cu (a) and the Al-Zn (b) binary alloys in the anolyte and catholyte solutions. The vertical dashed arrows indicate the filiform corrosion current value for each alloy.

A higher OCP for the Al-1.00Cu alloy both in the anolyte and in the catholyte compared with the Al-0.20Cu alloy is clear. The OCPs for the Al-0.20Cu and Al-1.00Cu alloys in the catholyte are respectively −0.77 V vs. SCE and −0.64 V vs. SCE. The pitting potential and the OCP for the Al-1.00Cu binary alloy in the anolyte appear to be very close at −0.73 and −0.75 V vs SCE respectively. For the Al-0.20Cu binary alloy in the anolyte the pitting potential and the OCP appear to be more distinct and to be at values of respectively −0.74 V vs SCE and −0.80 V vs SCE. The difference between the OCPs of the Al-1.00Cu in the anolyte and catholyte is higher than the OCP of the Al-0.20Cu in both electrolytes: respectively about 0.11 V and 0.03 V. Another important observation is that the Al-Cu alloys show an increase of the cathodic current in both the anolyte and the catholyte with increasing Cu concentration. For the degreased Al-Zn binary alloys the characteristic scans in both the anolyte and the catholyte are shown in Fig. 5b. The OCP values in the catholyte for the Al-Zn alloys show an increase from Al-0.19Zn to Al-0.48Zn, which is followed by a small drop in OCP from Al-0.48Zn to Al-0.97Zn and Al-2.09Zn. The OCP values in the anolyte show an overall small decrease of OCP with increasing Zn concentration. In contrast, the pitting potentials of these Al-Zn alloys in the anolyte show large variations and decrease with increasing Zn concentration. For the Al-0.19Zn the difference between the pitting potential and the OCP is the largest and this difference decreases with increasing Zn concentration: for the Al-2.09Zn alloy the pitting potential co-incides with the OCP. Another important observation is the decrease of cathodic current in the anolyte, resulting from the hydrogen reduction reaction, with increasing alloying concentration, unlike the observations on the Al-Cu alloys. The cathodic current in the catholyte only shows an initial increase in cathodic current from the Al-0.19Zn to the Al-0.48Zn sample but a further increase in Zn concentration yields little additional changes in the cathodic current in the catholyte. Furthermore, Fig. 5a and b show that if the cathode surface area is taken equal to the anode area (i.e. the catholyte curve shifts two orders of magnitude to the left because of the current surface area ratio of 100), the electrical current in the catholyte is always much lower than that in the anolyte at the same potential. This mainly originates from the availability of hydrogen ions in the anolyte.

4.5. Combination of potentiodynamic polarisation and filiform corrosion study

With the analysis of the filiform corrosion current as presented in Figs 5 and 6 one has to keep in mind that the filiform corrosion current in real filaments could differ significantly from the presented values, depending on the actual anodic and cathodic areas and the effective cathode/anode area ratio in real filaments. However, assuming a similar effective cathode/anode area ratio for the alloys investigated, the correlation between the filiform corrosion current and the filiform corrosion properties would still apply. Furthermore, the present

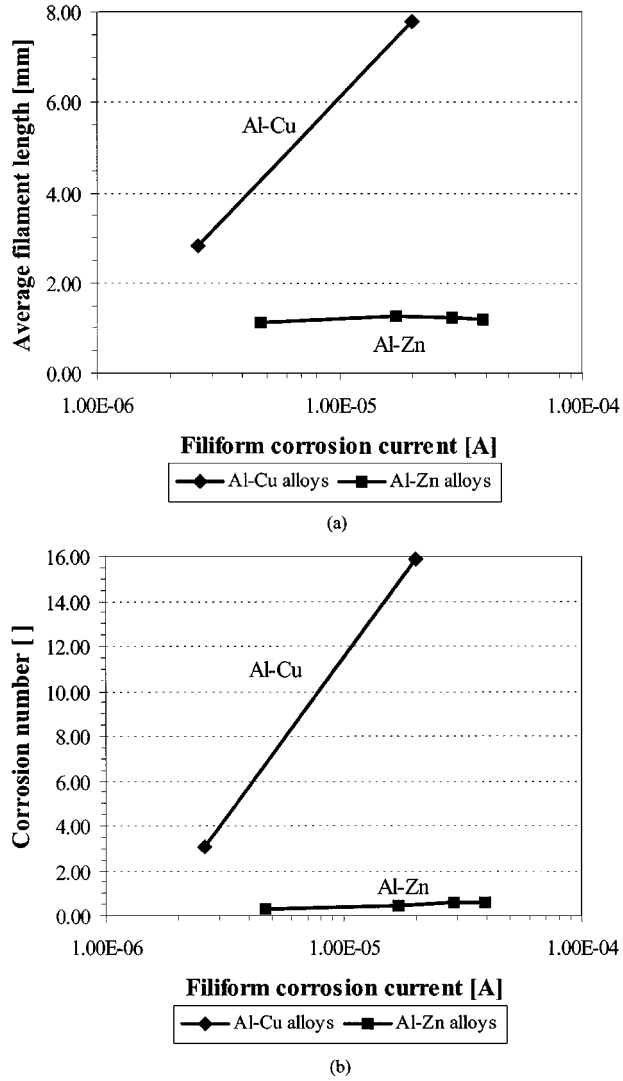

Figure 6 The correlation between the filiform corrosion current and the average filament length (a) and corrosion number (b) for the degreased Al-Cu binary alloys and the Al-Zn binary alloys.

analysis does not take into account the electrolytical resistance between the anodic and cathodic sites in real filaments. Lobry *et al.* [25] have shown for their system that the potential difference between anode and cathode of a macro differential aeration cell with an electrolytical connection is very small (∼10–20 mV) and very close to the OCP of the anode before the connection. This supports our present observations and incorporation of an electrolytical resistance into the model would not affect the correlation between the filiform corrosion current and the filiform corrosion properties.

The correlation between the filiform corrosion characteristics and filiform corrosion current is presented in Fig. 6 for the degreased Al-Cu and Al-Zn binary alloys. The filiform corrosion currents and relevant potentials are also summarised in Table II. It has to be noted that in the present analysis the filiform corrosion current is related to one-dimensional propagation rates of the filaments when filament width and in-depth attack are considered to be constant for comparable systems. Fig. 6a clearly shows that for the Al-Cu binary alloys a higher filiform corrosion current corresponds with a significantly higher average filament length after 1000 hours of accelerated exposure. This higher filiform corrosion

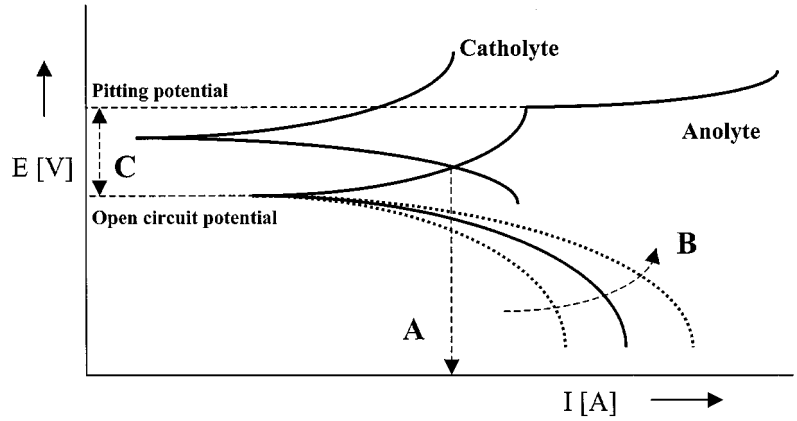

Figure 7 Schematic representation of the potentiodynamic polarisation curves in the anolyte and catholyte solutions. '**A**' indicates the position of the filiform corrosion current defined as the intercept of the cathodic curve in the catholyte and the anodic curve in the anolyte. Vector '**B**' indicates an increasing hydrogen reduction reaction rate in the anolyte and implicitly a higher sensitivity to local substrate composition variations. '**C**' indicates the passive range under anolyte conditions and herewith the filiform corrosion initiation characteristics of the alloy.

current also corresponds with an increasing Cu concentration in the alloy. These observations are in line with the investigation of Huisert *et al.* [26], who have reported an increasing filiform corrosion current with increasing average filament length for AA3000 series alloys. Although the samples and corresponding measurements can not be related directly, the corrosion currents found by Huisert *et al.* [26] are of the same order of magnitude as our filiform corrosion currents and in the range of 10^{-6}–10^{-5} A, assuming an effective cathode/anode area ratio of 100. Also the corresponding average filament lengths after 1000 hours of accelerated exposure test are similar and in the order of 1–10 mm. Such a relation of a higher filiform corrosion current corresponding with a higher average filament length is less clear for the less filiform corrosion susceptible Al-Zn binary alloys. The increasing filiform corrosion current is hardly reflected in an increasing average filament length for these alloys. The average lengths after 1000 hours of accelerated exposure test only vary from 1.14 to 1.25 mm, whereas the filiform corrosion currents vary from 4.7×10^{-6} to 3.9×10^{-5} A. Fig. 6b shows a very clear increase of the corrosion number with increasing filiform corrosion current and corresponding alloying concentration for the Al-Cu alloys. Although for the Al-Zn alloys a small absolute increase in corrosion number, 0.32 for the Al-0.19Zn to 0.60 for the Al-2.09Zn, with increasing filiform corrosion current is observed, the relative increase is deemed significant. As the average filament length is more or less constant for the Al-Zn alloys, the increase in corrosion number mainly reflects an increase in the filament site density. The clear increase in the filiform corrosion current mainly results from the changes in the anodic curves in the anolyte, i.e. while the cathodic curves in the catholyte do not show large differences (besides the initial increase from Al-0.19Zn to Al-0.48Zn), the pitting potential and the passive range decrease with Zn concentration as shown in Fig. 5b and Table II.

Further analysis of Fig. 6 shows that the higher average filament length and corrosion number for the Al-Cu alloys compared to those for the Al-Zn alloys with similar alloying concentrations are not reflected in a higher filiform corrosion current. When comparing the results for the Al-Cu and Al-Zn binary alloys it can be concluded that the correlation differs significantly with the solute atom and the filiform corrosion current turns out to be a non-uniquely discriminating parameter for the filiform corrosion susceptibility of the set of model alloys investigated. However, the observed relative filiform corrosion behaviour on Al-Cu and Al-Zn alloys can be rationalised by a more detailed analysis of the information in the potentiodynamic diagram shown schematically in Fig. 7 for a set of alloys. '**A**' indicates the position of the filiform corrosion current defined as the intercept of the cathodic curve in the catholyte and the anodic curve in the anolyte, as discussed in detail in the theoretical background section. Vector '**B**' indicates an increasing hydrogen reduction reaction rate in the anolyte and implicitly a higher sensitivity to local variations of substrate composition: these local variations can significantly influence the local potential values and herewith the local corrosion reaction rates. The length of vector '**C**' indicates the passive range under anolyte conditions which we relate to the filiform corrosion initiation characteristics: a smaller passive range corresponds to more rapid pitting and hence to a higher number of filiform corrosion initiations per scratch length, in this paper defined as the site density parameter.

We can now re-examine the electrochemical information in Fig. 5 and Table II. For the Al-Cu alloys the cathodic current in both the anolyte and the catholyte increases with the Cu concentration. This higher cathodic current, with an accompanying higher anodic dissolution rate, leads to a higher propagation rate, in line with the average filament length data. However, for the Al-Zn alloys an overall decrease of the cathodic current in the anolyte with increasing Zn concentration was observed in combination with a rather constant cathodic current in the catholyte. For this reason the filiform corrosion propagation rate is not likely to increase with increasing Zn concentration, which is again in line with the average filament length data from the present investigation, showing no significant differences in average filament lengths for the Al-Zn model alloys.

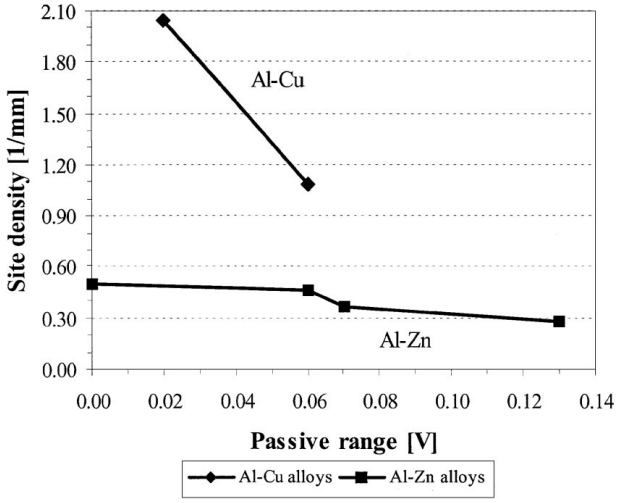

Figure 8 The site density for the degreased Al-Cu and Al-Zn model alloys as a function of the passive range in the anolyte.

For the Al-1.00Cu alloy the pitting potential was very close to the OCP, whereas the Al-0.20Cu showed a more distinct difference between the pitting potential and the OCP. If the ease of filiform corrosion initiation is related to the ease of pitting for a specific alloy, this would explain the higher site density for Al-1.00Cu compared to that for the Al-0.20Cu. The site density as a function of the passive range for both the Al-Cu and Al-Zn alloys is presented in Fig. 8. The increased ease of pitting will also enhance the propagation rate. The supposed correlation between ease of pitting and the ease of filiform corrosion initiation is also clear for the Al-Zn alloys. The reduction in passive range with increasing Zn concentration, corresponds to an increase of the site density, as presented in Fig. 8. This potentially easier pitting behaviour with increasing Zn concentration is not reflected in a higher propagation rate because of the opposing trends in cathodic current changes both in the catholyte and anolyte as a function of Zn concentration discussed above.

5. Conclusions

The accelerated filiform corrosion exposure tests show both a compositional and a pretreatment effect on the filiform corrosion behaviour of the tested substrates. For all tested degreased binary alloys, the site density increases with increasing concentration of the alloying element. The trend of an increasing average filament length with the alloying concentration is especially clear for the highly susceptible Al-Cu binary alloys and also for the degreased Al-Si alloys. This is in contrast with the degreased Al-Zn and Al-Mg alloys which show no or little significant increase in average filament length with solute content. Evaluation of the total filiform corrosion attack, defined as the product of the site density and the average filament length, shows that the average corrosion number decreases in the order Al-Cu, Al-Si, Al-Zn, Al-Mg. A further observation of the corrosion number data of the binary alloy system is that the corrosion number increases for all binary alloys with the alloying concentration. These observations support the applicability of the fundamental cause of local corrosion processes to filiform corrosion on aluminium alloys. Successive interactions between the alloy matrix and constituent particles are likely to be affected by the alloying elements and their concentrations. The trend of an increasing corrosion number with alloying concentration is particularly clear for the degreased samples. On the chromated and cerated samples the filiform corrosion attack was too small to confirm such a relation with any statistical significance, but the data would not contradict such a conclusion.

The results of the present set of experiments are in line with preceding investigations and a correlation between the polarisation measurements and both filiform corrosion propagation and total attack after the accelerated exposure test for the Al-Cu binary alloys is observed. Such a correlation is not observed for the Al-Zn alloys as an increasing filiform corrosion current is barely reflected in a higher average filament length. When comparing the results for the Al-Cu and Al-Zn binary alloys it can be concluded that the correlation differs significantly with the solute atom and the filiform corrosion current as defined turns out to be a non-uniquely discriminating parameter for the filiform corrosion susceptibility of the set of model alloys investigated in the present research. The different correlations for the Al-Cu and Al-Zn alloys are explained from the electrochemical response to local variations of the substrate composition. These local compositional variations will result in a higher overall cathodic and anodic reaction rate with increasing Cu concentration for the Al-Cu alloys. For the Al-Zn alloys a more constant overall cathodic and anodic reaction rate as a function of the Zn concentration is observed. This explains the increasing average filament length with Cu concentration and more constant average filament length with increasing Zn concentration after 1000 hours of accelerated exposure testing. For the Al-Cu and Al-Zn model alloys the filiform corrosion initiation characteristics are related to the passive range and thus implicitly to the ease of pitting of the alloy. A smaller passive range results in higher filiform site density for both the Al-Cu and Al-Zn alloys.

Acknowledgements

This project is financially supported by the Dutch Ministry of Economic Affairs, Innovation Oriented Research Program on Surface Technology (IOP-project IOT94001). Thanks are also due to Dr Scamans and Mr Afseth for supplying the aluminium model alloys, Ms Nelson and Mr Grey for their technical contributions to this work and Dr Tony Hughes, Dr Ken Lai, Dr Erik van Westing and Mr Martin Huisert for the helpful discussions.

References

1. H. J. W. LENDERINK, PhD thesis, Delft University of Technology, The Netherlands, 1995.
2. G. M. BROWN, K. SHIMIZU, K. KOBAYASHI, G. E. THOMPSON and G. C. WOOD, *Corr. Sci.* **34** (1993) 1045.

3. CHI-MIN LIAO, J. M. OLIVE, MING GAO and R. P. WEI, *Corrosion* **54** (1998) 451.
4. CHI-MIN LIAO, G. S. CHEN and R. P. WEI, *Scripta Mater.* **35** (1996) 1341.
5. "Metals Handbook, Vol. 13: Corrosion," 9th ed., (ASM International, Metals Park, OH, 1987) p. 113.
6. Z. SZKLARASKA-SMIALOWSKA, *Corrosion* **27** (1971) 223.
7. J. ZAHAVI and M. METZGER, in "Localized Corrosion," edited by R. W. Staehle, B. F. Brown, J. Kruger and A. Agrawal, 1974, p. 547. International Conf. Series, NACE-3, Houston, TX, December 10–16 1971.
8. G. S. CHEN, M. GAO, D. G. HARLOW and R. P. WEI, in FAA/NASA Int. Symp. on Advanced Structural Integrity Methods for Airframe Durability and Damage Tolerance, Langley Research Center, Hampton, VA, September 1994, NASA Conference Publication 3274, p. 157.
9. G. S. CHEN, M. GAO and R. P. WEI, *Corrosion* **52** (1996) 8.
10. M. IWATA, M. NISHIKADO, E. SATO and Y. ITOI, *Jap. Inst. Metals* **34** (1984) 531.
11. K. NISCANCIOGLU, H. LETH-OLSEN and O. LUNDER, "Corrosion Protection by Organic Coatings," (Cambridge, UK, 1994) p. 40.
12. Y. KOMATSU, E. SUZUKI, K. MIYAZAKI and T. NISHINO, in SAE, Detroit, USA paper 910887, 1991.
13. H. A. KATZMAN and G. M. MALOUF, *Appl. of Surface Sci.* **2** (1979) 416.
14. D. J. McCOY, in Proceedings 2nd AESF/EPA Chromium Colloquium, Miami, FL, February 1990.
15. D. R. ARNOTT, B. R. W. HINTON and N. E. RYAN, *Corrosion* **45** (1989) 12.
16. F. MANSFELD, S. LIN, S. KIM and H. SHIH, *ibid.* **45** (1989) 615.
17. A. J. DAVENPORT, H. S. ISAACS and M. W. KENDIG, *Corr. Sci.* **32** (1991) 653.
18. A. J. ALDYKIEWICZ, H. S. ISAACS and A. J. DAVENPORT, *J. Electrochem. Soc.* **142** (1995) 3342.
19. A. E. HUGHES, K. J. NELSON, R. J. TAYLOR, B. R. W. HINTON, M. J. HENDERSON, L. WILSON and S. A. NUGENT, International Patent Appl. No. PCT/AU94/00539, International Patent No. WO95/08008.
20. B. R. W. HINTON, D. R. ARNOTT and N. E. RYAN, *Metals Forum* **7** (1984) 211.
21. D. R. ARNOTT, N. E. RYAN, B. R. W. HINTON, B. A. SEXTON and A. E. HUGHES, *Appl. Surface Sci.* **22/23** (1985) 236.
22. A. E. HUGHES, R. J. TAYLOR, B. R. W. HINTON and L. WILSON, *Surface and Interface Analysis* **23** (1995) 540.
23. H. KAESCHE, *Werkstoffe und Korrosion* **11** (1959) 668.
24. D. H. VAN DER WEIJDE, E. P. M. VAN WESTING and J. H. W. DE WIT, *Electrochim. Acta* **41** (1996) 1103.
25. V. LOBRY, S. VANDEPUTTE and J. VEREECKEN, in Proceedings Eurocorr '98 Conference Working Party 14 Coatings, Utrecht, The Netherlands, September 28–October 1, 1998.
26. M. H. M. HUISERT, D. H. VAN DER WEIJDE, J. H. W. DE WIT and L. KATGERMAN, in Proceedings Eurocorr '98 Conference Working Party 14 Coatings, Utrecht, The Netherlands, September 28–October 1, 1998.
27. T. H. NGUYEN and R. T. FOLEY, *J. of Electrochem. Soc.* **127** (1980) 2563.
28. W. H. SLABAUGH, W. DEJAGER, S. E. HOOVER and L. L. HUTCHINSON, *J. of Paint Techn.* **44** (1972) 76.
29. G. M. HOCH and R. F. TOBIAS, NACE Corrosion/71 paper no. 19, 1971.
30. M. G. FONTANA and N. D. GREENE, "Corrosion Engineering" (McGraw-Hill Book Company, USA, 1967) p. 314.
31. G. M. HOCH, in NACE 1974, Vol. 3, 1974, p. 134.
32. Deutsches Institut Für Normung e.V., Number 65472: Filiform corrosion test of coatings on aluminium alloys, draft, 1989.
33. R. QVARFORT, *Corr. Sci.* **28** (1988) 135.
34. G. M. SCAMANS, M. P. AMOR, B. R. ELLARD and J. A. HUNTER, in Proceedings AlSST '97 Symposium, Antwerp, Belgium, May 12–15 1997, p. 229.
35. D. C. M. WILMS, Internal Report, Delft University of Technology, The Netherlands, 1996.

Received 10 March
and accepted 22 October 1999